Supporting Information

for

Industrially promising NiCoP nanorod arrays tailored with trace W and Mo atoms for boosting large-current-density overall water splitting

Xin Guo,‡ Menggang Li,‡ Lin He, Shuo Geng, Fenyang Tian, Ying Song, Weiwei Yang*, Yongsheng Yu*

MIIT Key Laboratory of Critical Materials Technology for New Energy Conversion and Storage, School of Chemistry and Chemical Engineering, Harbin Institute of Technology, Harbin, Heilongjiang 150001, China

‡ These authors contributed equally.

E-mail address: yangww@hit.edu.cn (W. Yang); ysyu@hit.edu.cn (Y. Yu)

Experimental Section

Chemicals and materials.

The Ni foam (NF) was purchased from Kunshan Jiayisheng Electronics Co., Ltd (China). $Co(NO_3)_2 \cdot 6H_2O$, NH_4F, $CO(NH)_2$, Na_2WO_4, Na_2MoO_4, KOH, HCl and ethanol were all purchased from Aladdin. All chemicals with analytical grade were directly used without further purification. All solutions were freshly prepared with ultrapure water (18.2 MΩ/cm).

Synthesis of W,Mo co-doped NiCoP nanorod arrays (W,Mo-NiCoP/NF)

A piece of NF was first carefully sonicated in acetone, 1 M HCl, deionized water and ethanol for 15 min to clean the surface, respectively. Firstly, W,Mo-NiCo precursor/NF was synthesized by the hydrothermal process. Typically, $Co(NO_3)_2 \cdot 6H_2O$ (0.98 mmol), Na_2MoO_4 (0.01 mmol), Na_2WO_4 (0.01 mmol), $Co(NH_2)_2$ (6.00 mmol) and NH_4F (1.00 mmol) were dissolved in 30 mL of deionized water to form a pink solution. As-obtained pink solution with treated NF was transferred to 50 mL Teflon-lined stainless-steel autoclave and heated at 120 °C for 6 h. Then, the precursor was collected, washed with deionized water and ethanol for several times and dried in vacuum overnight. Secondly, the W,Mo-NiCo precursor/NF was converted to W,Mo-NiCoP/NF by the phosphation process. The as-prepared precursor and 0.5 g of $NaH_2PO_2 \cdot H_2O$ were placed at both ends of a tubular furnace, and $NaH_2PO_2 \cdot H_2O$ was at the upstream side. The phosphation process was conducted at 300 °C for 2 h with a heating rate of 2 °C min^{-1} under continuous Ar flow. To optimize the amount of doping Mo atoms, different contents of Na_2MoO_4 (0.01, 0.02 and 0.05 mmol) were conducted to synthesize various Mo doped bimetallic phosphides (shortly named as 1%, 2%, 5% Mo-NiCoP/NF). The optimized amount of W atoms (1%, 2%, 5% W-NiCoP/NF) and W, Mo co-doping amount (1%, 2.5%, 5% W,Mo-NiCoP/NF) were achieved except using different amount of Na_2MoO_4 or Na_2WO_4. For comparison, Pt/C and Ir/C were coated on Ni foam with the same loading amount as the above samples.

Material characterizations

The crystal phases were determined by X-ray diffraction (XRD) on a PAN analytical X'Pert Powder with Cu Kα radiation (λ = 1.5418 Å). The morphology, composition and microstructure of the as-obtained electrodes were characterized by scanning electron microscopy (SEM, JEOL JSM-6360) with energy dispersive X-ray spectrometry (SEM-EDS), transmission electron microscopy (TEM, JEM-1500 operated at 100 kV) and high-resolution TEM (HRTEM, Tecnai G2 F30). The elemental specials of the products were measured by X-ray photoelectron spectroscopy (XPS, Thermo ESCALAB250Xi).

Electrochemical measurements

All the electrochemical tests were performed on a CHI760E electrochemical station. Both HER and OER were measured in a three-electrode configuration using 1.0 M KOH as electrolyte. The Ni foam with active nanorod arrays was directly employed as the working electrode in electrochemical measurement, while the graphite bar and saturated calomel electrode (SCE) electrodes were used as the counter and reference electrodes, respectively. The polarization curves were recorded at a scan rate of 2 mV s^{-1} and were compensated with iR correction. Reference electrode values were calculated via E(RHE) = E(SCE) + 0.241 + 0.059 × pH. Electrochemical impedance spectroscopy (EIS) tests were conducted in the frequency range from 0.01 Hz to 100 kHz. The multi-chronoamperometric and chronopotentiometric curves were recorded at a broad potential and a constant potential without IR-compensation. Electrochemical surface area (ESCA) was examined by double-layer capacitance (C_{dl}) measurements by unequal scan rates (20, 40, 60, 80, 100 and 120 $mV \cdot s^{-1}$).

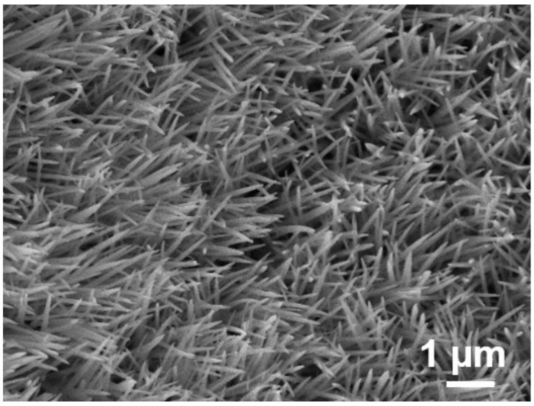

Figure S1. SEM image of W,Mo-NiCo-precursor/NF.

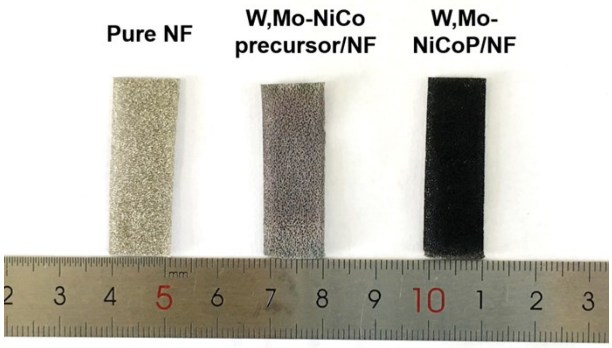

Figure S2. Optical images of pure NF, W,Mo-NiCo precursor/NF and W,Mo-NiCoP/NF.

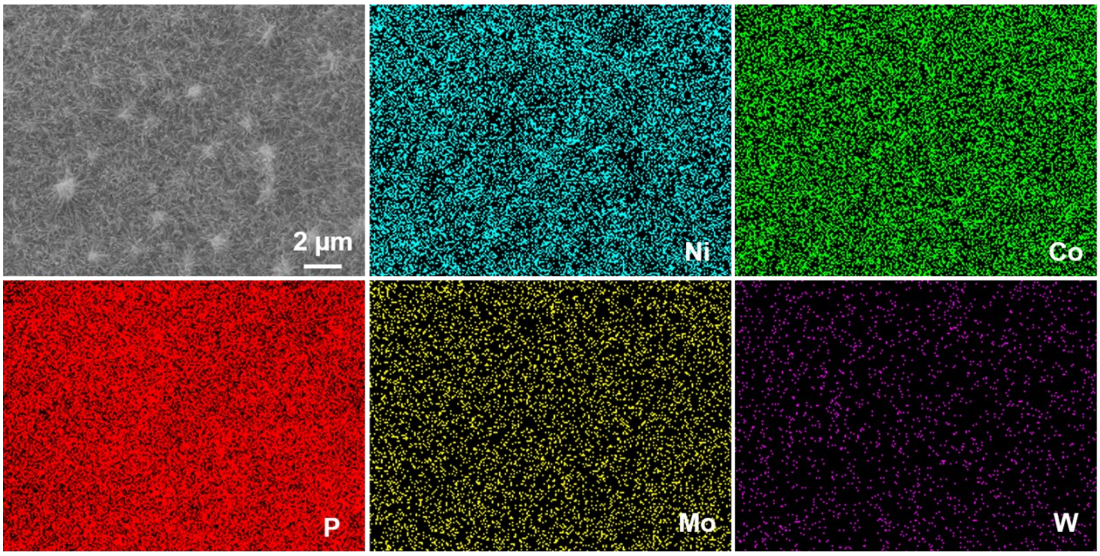

Figure S3. EDS mapping of W,Mo-NiCoP/NF.

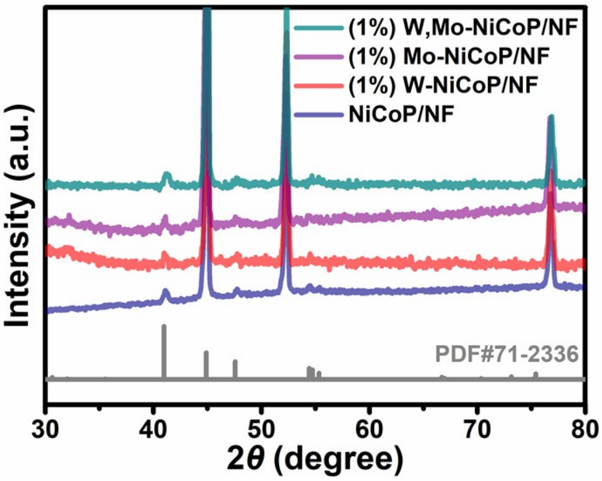

Figure S4. XRD patterns of (1%) W,Mo-NiCoP/NF, (1%) Mo-NiCoP/NF, (1%) W-NiCoP/NF and NiCoP/NF.

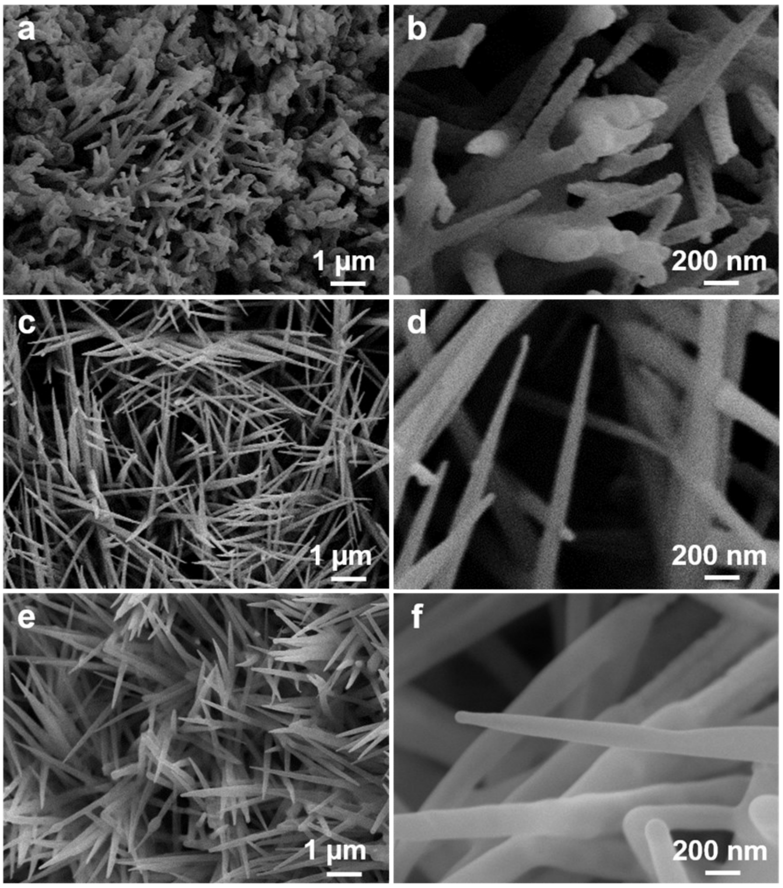

Figure S5. SEM images of (a,b) Mo-NiCoP/NF, (c,d) W-NiCoP/NF and (e,f) NiCoP/NF.

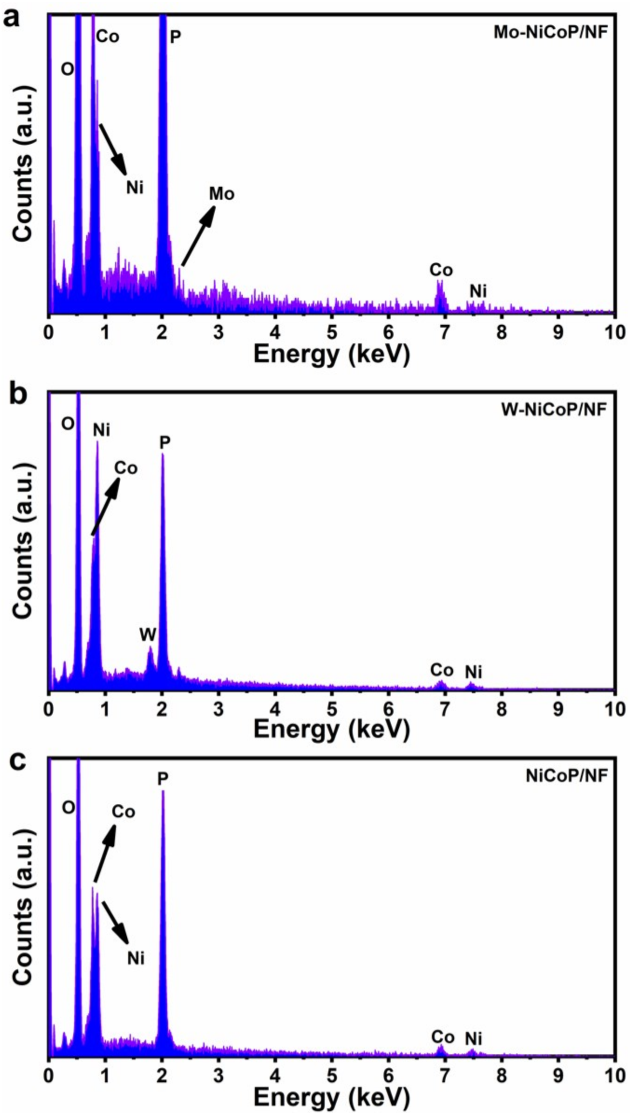

Figure S6. EDS spectra of (a) Mo-NiCoP, (b) W-NiCoP and (c) NiCoP/NF.

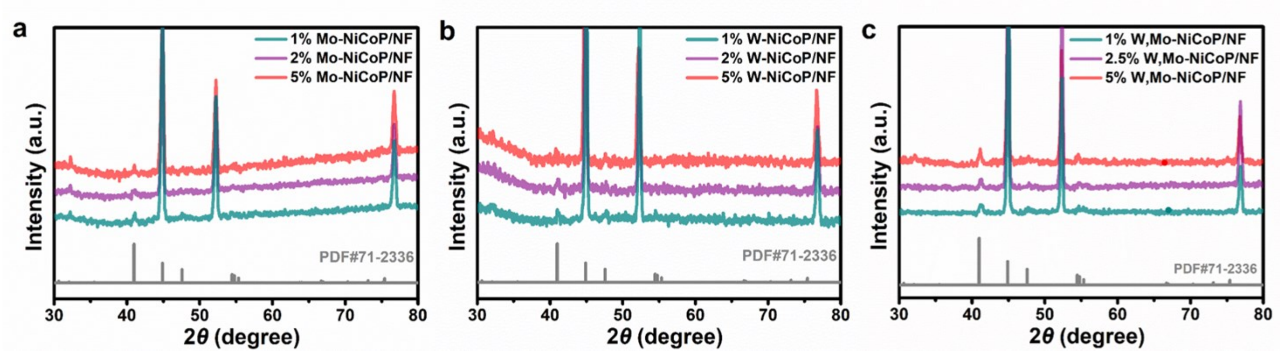

Figure S7. XRD patterns of (a) Mo-NiCoP, (b) W-NiCoP and (c) W, Mo-NiCoP/NF with different doping amount of W/Mo atoms.

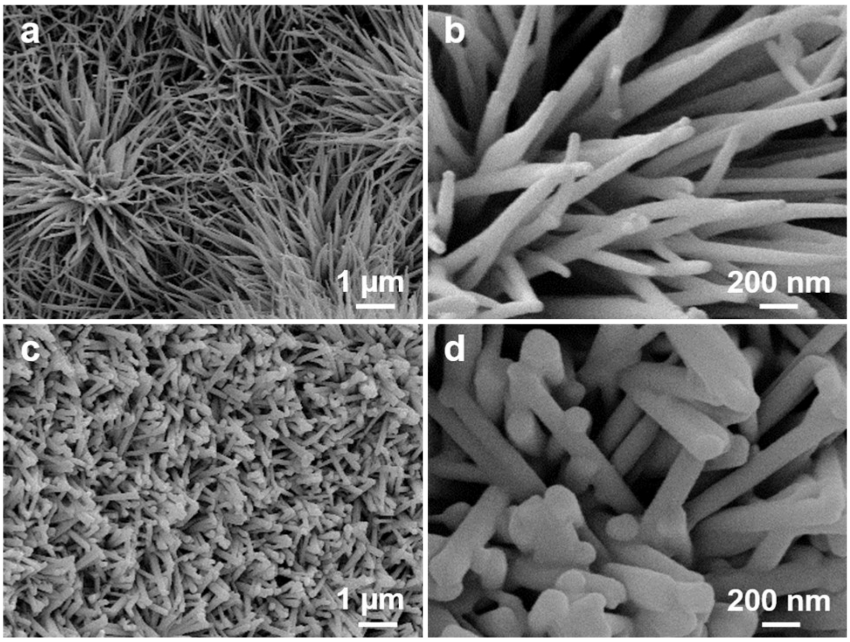

Figure S8. SEM images of (a,b) 2% Mo-NiCoP/NF and (c,d) 5% Mo-NiCoP/NF.

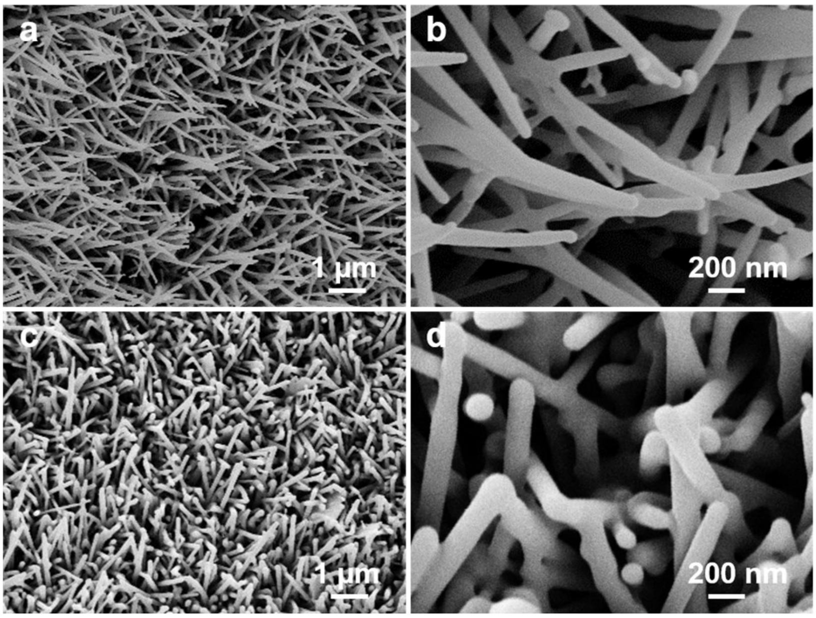

Figure S9. SEM images of (a,b) 2% W-NiCoP/NF and (c,d) 5% W-NiCoP/NF.

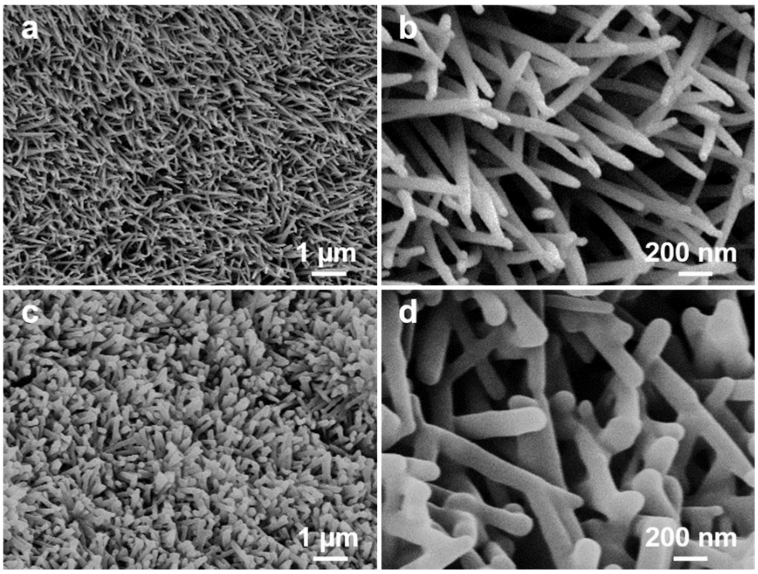

Figure S10. SEM images of (a,b) 2.5% W,Mo-NiCoP/NF and (c,d) 5% W,Mo-NiCoP/NF.

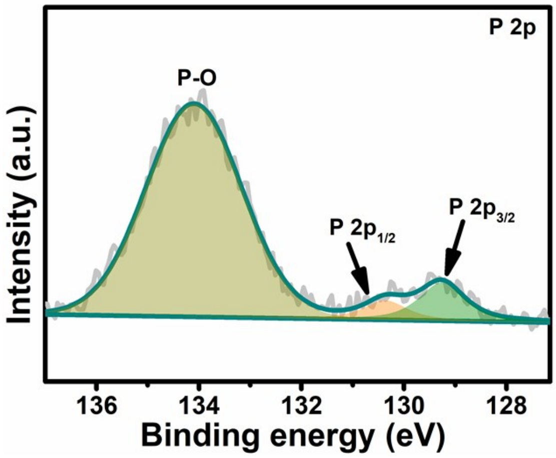

Figure S11. XPS spectrum of P 2p in W,Mo-NiCoP/NF.

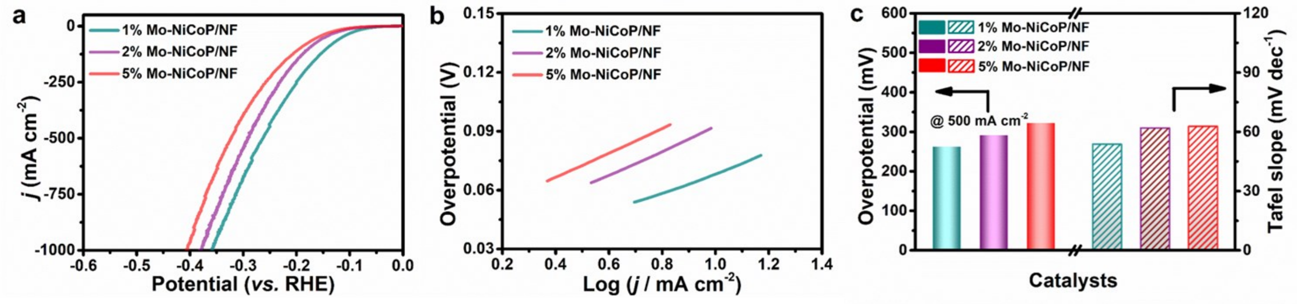

Figure S12. HER performance of all as-synthetized Mo-NiCoP/NF. (a) The HER polarization curves, (b) the corresponding Tafel slope plots, (c) the overpotentials at a large current density of 500 mA cm^{-2} (left) and the corresponding Tafel slopes (right).

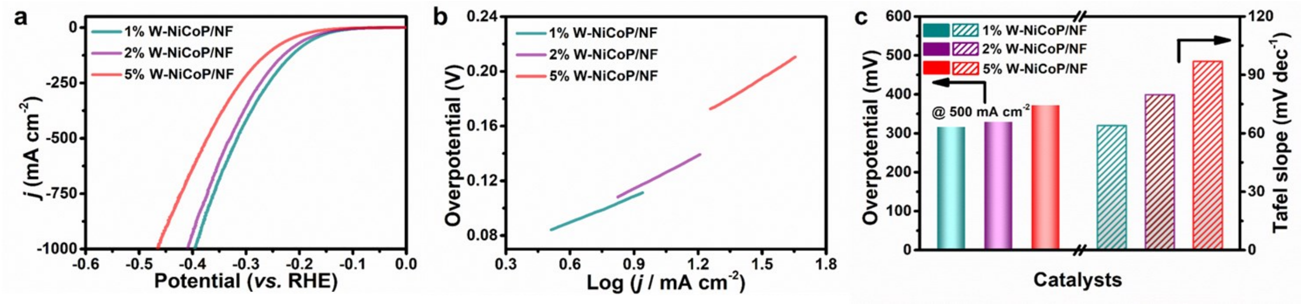

Figure S13. HER performance of all as-synthetized W-NiCoP/NF. (a) The HER polarization curves, (b) the corresponding Tafel slope plots, (c) the overpotentials at a large current density of 500 mA cm^{-2} (left) and the corresponding Tafel slopes (right).

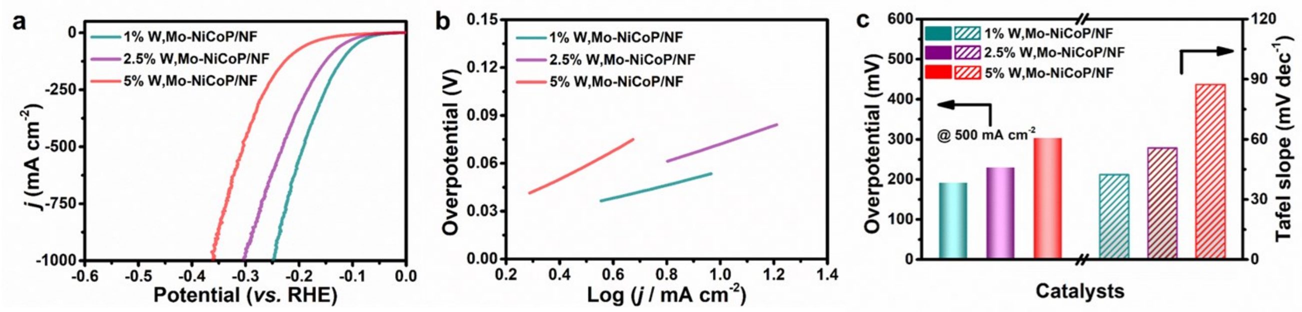

Figure S14. HER performance of all as-synthetized W, Mo-NiCoP/NF. (a) The HER polarization curves, (b) the corresponding Tafel slope plots, (c) the overpotentials at a large current density of 500 mA cm^{-2} (left) and the corresponding Tafel slopes (right).

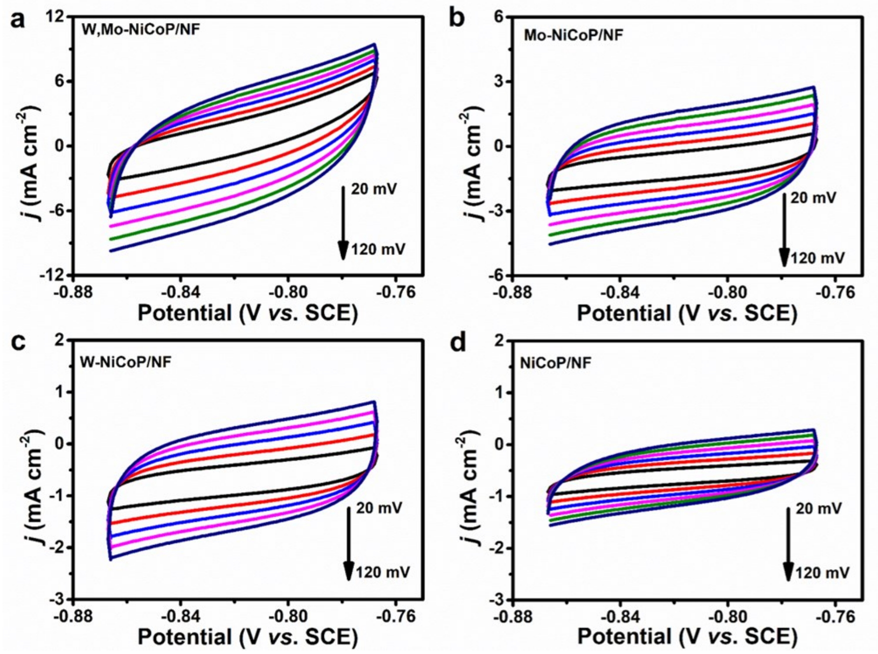

Figure S15. Cyclic voltammetry curves with different scan rates of (a) W,Mo-NiCoP/NF, (b) Mo-NiCoP/NF, (c) W-NiCoP and (d) NiCoP/NF.

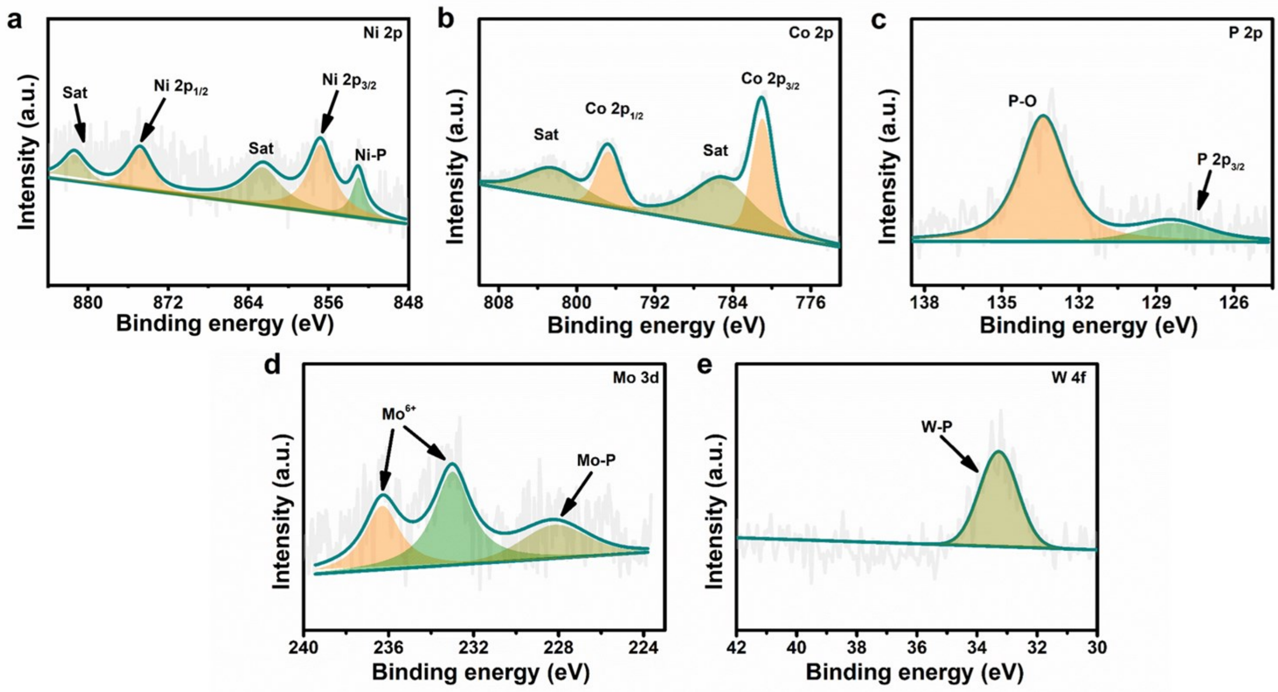

Figure S16. XPS spectra of W, Mo-NiCoP/NF after long-time HER tests. (a) Ni 2p, (b) Co 2p, (c) P 2p, (d) Mo 3d and (e) W 4f.

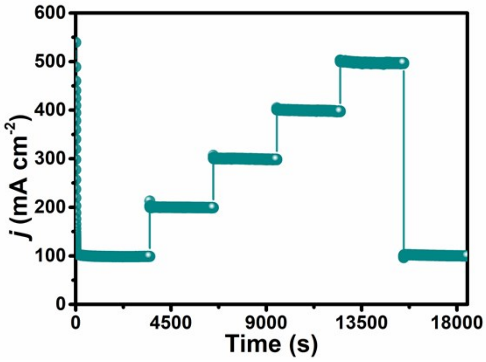

Figure S17. Multi-chronoamperometric response curve of W,Mo-NiCoP/NF for OER.

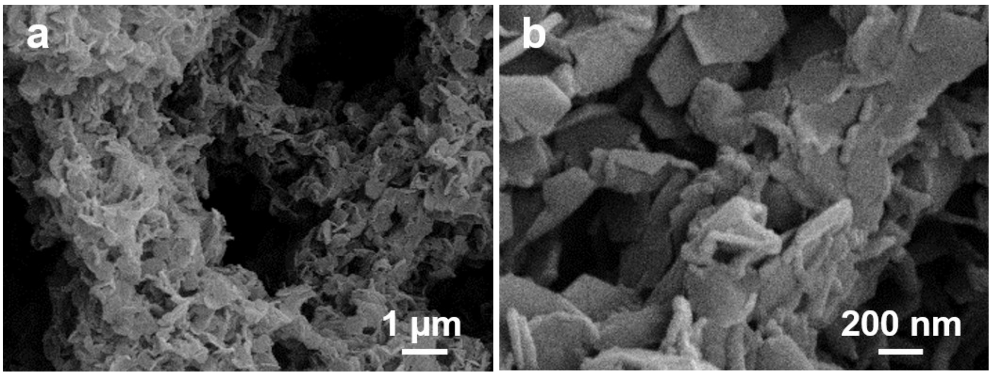

Figure S18. (a) low- and (b) high-magnification SEM images of W,Mo-NiCoP/NF after long-time OER tests.

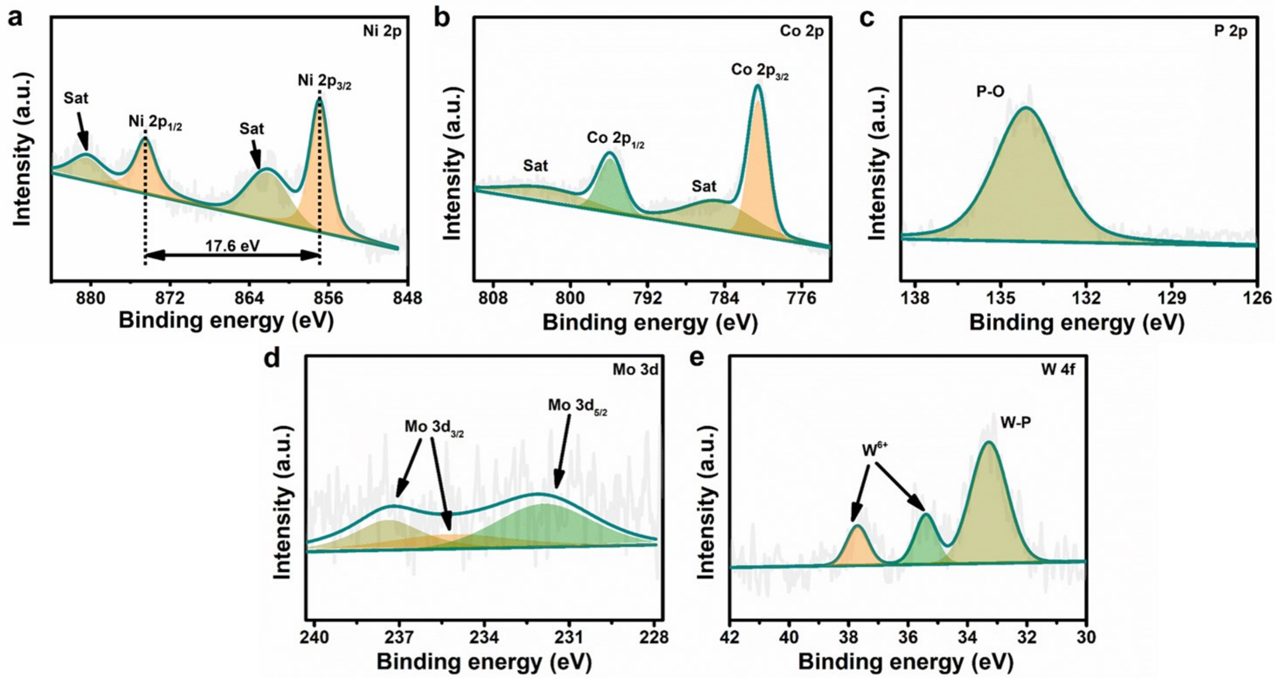

Figure S19. XPS spectra of W,Mo-NiCoP/NF after long-time OER tests. (a) Ni 2p, (b) Co 2p, (c) P 2p, (d) Mo 3d and (e) W 4f.

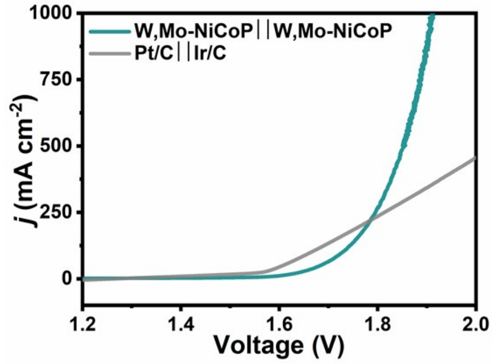

Figure S20. Polarization curves towards overall water splitting.

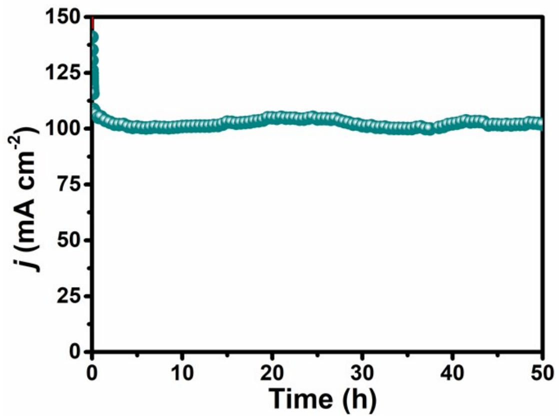

Figure S21. Chronopotentiometric curve of W,Mo-NiCoP/NF || W,Mo-NiCoP/NF for overall water splitting.

Table S1. The elemental composition of samples from ICP-OES.

	Co Atomic %	**Mo Atomic %**	**W Atomic %**
W,Mo-NiCoP/NF	97.828%	1.099%	1.072%
Mo-NiCoP/NF	98.870%	1.089%	——
W-NiCoP/NF	98.985%	——	1.015%

Table S2. Comparison of HER performances for W,Mo-NiCoP/NF with state-of-the-art electrocatalysts *yet* reported in the alkaline media.

Electrocatalysts	**Overpotential @ Current density**	**Reference**
$Ni_{1.8}Cu_{0.2}$-P/NF[1]	78 mV @10 mA cm^{-2} 245 mV @100 mA cm^{-2}	Appl. Catal. B-Environ. 243 (2019) 537-545.
$Ni_{12}P_5$-Ni_2P	129 mV @ 10 mA cm^{-2} 202 mV @ 100 mA cm^{-2}	Appl. Catal. B-Environ. 282 (2021) 119609.
CoP film/Ti substrate	86 mV @ 10 mA cm^{-2} 376 mV @ 150 mA cm^{-2}	Adv. Energy Mater. 8 (2018) 1802445.
$Ni_{2(1-x)}Mo_{2x}P$	72 mV @ 10 mA cm^{-2} 162 mV @ 100 mA cm^{-2} 240 mV @ 500 mA cm^{-2} 294 mV @ 1000 mA cm^{-2}	Nano Energy 53 (2018) 492-500.
Co/CoO@NC@CC[2]	152 mV @ 10 mA cm^{-2} 232 mV @ 100 mA cm^{-2}	Chem. Eng. J. 414 (2021) 128804.
Fe-Ni_2P@PC/Cu_xS[3]	□112.9 mV @ 10 mA cm^{-2}	Nano Energy 84 (2021) 105861.
NiFe LDH@NiCoP	120 mV @ 10 mA cm^{-2} 320 mV @ 100 mA cm^{-2}	Adv. Funct. Mater. 28 (2018) 1706847.
A-$NiSe_2$|P	111 mV @ 10 mA cm^{-2} 187 mV @ 100 mA cm^{-2}	J. Colloid Interface Sci. 571 (2020) 260-266.
Ni_3N-VN/NF[1]	218 mV @ 100 mA cm^{-2}	Adv. Mater. 31 (2019) 1901174.
F-Co_2P/Fe_2P/IF[4]	229.8 mV @ 500 mA cm^{-2}	Chem. Eng. J. 399 (2020) 125831.
A-NiCo LDH/NF[1]	286 mV @ 500 mA cm^{-2} 381 mV @ 1000 mA cm^{-2}	Appl. Catal. B-Environ. 261 (2020) 118240.
NFN-MOF/NF[1]	293 mV @ 500 mA cm^{-2}	Adv. Energy Mater. 8 (2018) 1801065.
$Fe_{13.7\%}$-Ni_3S_2	246 mV @ 500 mA cm^{-2}	ChemElectroChem 6 (2019) 4550-4559.
Ni_2P/NF[1]	306 mV @ 1000 mA cm^{-2}	J. Am. Chem. Soc. 141 (2019) 7537-7543.
W,Mo-NiCoP/NF[1]	**55 mV @ 10 mA cm^{-2}** **114 mV@ 100 mA cm^{-2}** **192 mV@ 500 mA cm^{-2}** **249 mV @ 1000 mA cm^{-2}**	**This work**

[1-4] NF, CC, PC, IF were denoted as the nickel foam, carbon cloth, P-doped porous carbon and iron foam, respectively.

Table S3. Comparison of overall water splitting performance in 1 M KOH electrolyte between W,Mo-NiCoP/NF and state-of-the-art bifunctional electrocatalysts *yet* reported

Water alkaline electrolyzer	Cell voltage@ Current density	Reference
Co-Ni-P	1.64 V @ 10 mA cm^{-2}	Chem. Eng. J. 420 (2021) 129686.
Cu_1Ni_2-N	1.63 V @ 10 mA cm^{-2}	Adv. Energy Mater. 9 (2019) 1900390.
$Co_5Mo_{1.0}O$ NSs@NF	1.68 V @ 10 mA cm^{-2} 1.89 V @ 100 mA cm^{-2}	Nano Energy 45 (2018) 448-455.
Co-Mo_2C-CN_x-2	1.68 V @ 10 mA cm^{-2}	Appl. Catal. B-Environ. 284 (2021) 119738.
Co/CoO@NC@CC	1.66 V @ 10 mA cm^{-2}	Chem. Eng. J. 414 (2021) 128804.
Fe-Ni_2P@PC/Cu_xS	1.62 V @ 10 mA cm^{-2}	Nano Energy 84 (2021) 105861.
CoP NFs	1.65 V @ 10 mA cm^{-2}	ACS Catal. 10 (2020) 412-419.
CoFeZr oxides/NF	1.64 V @ 10 mA cm^{-2}	Adv. Mater. 31 (2019) 1901439.
Co_2P/CoP	1.65 V @ 10 mA cm^{-2}	J. Power Sources. 402 (2018) 345-352.
Co-NC@Mo_2C	1.685 V @ 10 mA cm^{-2}	Nano Energy 57 (2019) 746-752.
A-$NiSe_2$|P	1.62 V @ 10 mA cm^{-2} 1.78 V @ 100 mA cm^{-2}	J. Colloid Interface Sci. 571 (2020) 260-266.
NiCoP@NF-100	1.80 V @ 100 mA cm^{-2}	J. Energy Chem. 50 (2020) 395-401.
Mo-Ni_3S_2/Ni_xP_y/NF	1.80 V @ 100 mA cm^{-2}	Adv. Energy Mater. 10 (2020) 1903891.
N-Ni_3S_2/NF	1.815 V @ 100 mA cm^{-2}	Adv. Mater. 29 (2017) 1701584.
Ni-ZIF/Ni-B/NF	1.78 V @ 100 mA cm^{-2}	Adv. Energy Mater. 10 (2020) 1902714.
NiFe LDH@NiCoP/NF	1.90 V @ 100 mA cm^{-2}	Adv. Funct. Mater., 2018, 28, 1706847.
$NiCo_2S_4$/NF	1.94 V @ 100 mA cm^{-2}	Adv. Funct. Mater. 29 (2019) 1807031.
$Ni_xCo_{3-x}S_4$/Ni_3S_2	1.80 V @ 100 mA cm^{-2}	Nano Energy 35 (2017) 161-170.
$Fe_{13.7\%}$-Ni_3S_2	1.95 V @ 500 mA cm^{-2}	ChemElectroChem 6 (2019) 4550-4559.
NFN-MOF/NF	1.96 V @ 500 mA cm^{-2}	Adv. Energy Mater. 2018, 8, 1801065.
Fe-FVO-60-act	1.88V @ 500 mA cm^{-2}	Chem. Eng. J. 416 (2021) 129165.
P-MoS_2@CoP	1.94V @ 500 mA cm^{-2}	ChemSusChem 14 (2021) 1565-1573.
W,Mo-NiCoP/NF	**1.59 V @10 mA cm^{-2}** **1.74 V @ 100 mA cm^{-2}** **1.85 V @ 500 mA cm^{-2}**	**This work**

NF was denoted as nickel foam in this table.